Draft version October 11, 2010
Preprint typeset using LaTeX style emulateapj v. 05/04/06

HOW UNIVERSAL IS THE $\Sigma_{\rm SFR} - \Sigma_{\rm H_2}$ RELATION?

R. Feldmann[1,2], N. Y. Gnedin[1,2,3] and Andrey V. Kravtsov[2,3,4]

Draft version October 11, 2010

ABSTRACT

It is a well established empirical fact that the surface density of the star formation rate, $\Sigma_{\rm SFR}$, strongly correlates with the surface density of molecular hydrogen, $\Sigma_{\rm H_2}$, at least when averaged over large ($\sim$ kpc) scales. Much less is known, however, if (and how) the $\Sigma_{\rm SFR} - \Sigma_{\rm H_2}$ relation depends on environmental parameters, such as the metallicity or the UV radiation field in the interstellar medium (ISM). Furthermore, observations indicate that the scatter in the $\Sigma_{\rm SFR} - \Sigma_{\rm H_2}$ relation increases rapidly with decreasing averaging scale. How the scale dependent scatter is generated and how one recovers a tight $\sim$ kpc scale $\Sigma_{\rm SFR} - \Sigma_{\rm H_2}$ relation in the first place is still largely debated. Here, we explore these questions with hydrodynamical simulations that follow the formation and destruction of H_2, include radiative transfer of UV radiation, and resolve the ISM on ~ 60 pc scales. We find that within the considered range of H_2 surface densities (10-100 $M_\odot$ pc^{-2}) the $\Sigma_{\rm SFR} - \Sigma_{\rm H_2}$ is steeper in environments of low metallicity and/or high radiation fields (compared to the Galaxy), that the star formation rate at a given H_2 surface density is larger, and the scatter is increased. We expect that deviations from a "universal" $\Sigma_{\rm SFR} - \Sigma_{\rm H_2}$ relation should be particularly relevant for high redshift galaxies or for low-metallicity dwarfs at $z \sim 0$. We also find that the use of time-averaged SFRs produces a large, *scale dependent* scatter in the $\Sigma_{\rm SFR} - \Sigma_{\rm H_2}$ relation. Therefore, one does not necessarily need to invoke a changing star formation efficiency over the life time of molecular clouds in order to explain it. Given the plethora of observational data expected from upcoming surveys such as ALMA the scale-scatter relation may indeed become a valuable tool for determining the physical mechanisms connecting star formation and H_2 formation.

Subject headings: galaxies: evolution — stars: formation — methods: numerical

1. INTRODUCTION

In a seminal paper Schmidt (1959) constructed a closed-box model of gas consumption and star formation that relies on the basic assumption of a polynomial relationship between (total) gas surface density $\Sigma_{\rm gas}$ and star formation rate surface density $\Sigma_{\rm SFR}$. This model was able to satisfy simultaneously a number of observational constraints, such as the initial luminosity function of main sequence stars, the luminosity function of white dwarfs, or the relatively constant surface density of atomic hydrogen (HI). While the first studies focussed on the relation between neutral hydrogen and SFR (Sanduleak 1969; Hartwick 1971), the combination of measurements of Hα, HI and CO emission lines allowed for a direct test of the Schmidt relation, $\Sigma_{\rm SFR} - \Sigma_{\rm gas}$, and a precise measurement of its exponent (Kennicutt 1989, 1998b). Initially, it was assumed that $\Sigma_{\rm gas}$ would determine $\Sigma_{\rm SFR}$ (e.g., via gravitational collapse). However, measurements of azimuthally averaged gas and SFR profiles showed that SFRs correlate better with the *molecular* hydrogen (H_2) component than with the *total* gas density (Wong & Blitz 2002; Bigiel et al. 2008). In fact, recent observational and theoretical works demonstrate that the $\Sigma_{\rm SFR} - \Sigma_{\rm gas}$ relation steepens at low gas surface densities due to the transition of atomic to molecular hydrogen (Robertson & Kravtsov 2008; Bigiel et al. 2008; Krumholz et al. 2009b; Gnedin & Kravtsov 2010a). The shape of the $\Sigma_{\rm SFR} - \Sigma_{\rm gas}$ relation is also predicted to evolve strongly with redshift due to the build-up of metallicity in the interstellar medium (ISM) over cosmic history and the importance of dust in the formation of H_2 and its shielding from Lyman-Werner radiation (Krumholz et al. 2009a; Gnedin & Kravtsov 2010b). In contrast, the $\Sigma_{\rm SFR} - \Sigma_{\rm H_2}$ relation is often assumed to evolve little and be relatively insensitive to changes in metallicity and interstellar radiation field, although this has not yet been confirmed observationally. The assumption on which this "universality" is based is that the efficiency with which clouds of molecular hydrogen convert their H_2 into stars is not a strong function of the average ISM metallicity or the interstellar radiation field, at least under conditions typical for spiral galaxies (Krumholz & Tan 2007). The scale at which this conversion takes place is the scale of (giant) molecular clouds, i.e. 100 pc or less. However, there are a couple of complications. First, there is growing observational evidence suggesting that the scatter in the $\Sigma_{\rm SFR} - \Sigma_{\rm H_2}$ relation increases if one goes to smaller and smaller scales (see, e.g., Onodera et al. 2010; Schruba et al. 2010). Taken at face value this seems to contradict a tight small-scale coupling between molecular hydrogen surface density and star formation. Second, the $\Sigma_{\rm SFR} - \Sigma_{\rm H_2}$ relation is typically measured on $\sim$ kpc scales and the spatial averaging may lead to changes in the slope, intercept and scatter compared with those on small scales (Kravtsov 2003). Third, observationally determined SFRs are time-averaged over the effective lifetime of the specific star formation tracer and may thus differ from instantaneous SFRs.

[1] Center for Particle Astrophysics, Fermi National Accelerator Laboratory, Batavia, IL 60510, USA; feldmann@fnal.gov
[2] Kavli Institute for Cosmological Physics, The University of Chicago, Chicago, IL 60637 USA
[3] Department of Astronomy & Astrophysics, The University of Chicago, Chicago, IL 60637 USA
[4] Enrico Fermi Institute, The University of Chicago, Chicago, IL 60637

A straightforward observational check of the universality of the $\Sigma_{\rm SFR} - \Sigma_{\rm H_2}$ relation is difficult, first and foremost because the direct detection of molecular hydrogen is challenging. Tracer molecules such as CO or HCN are typically used instead to infer the H_2 column density (Omont 2007). Mapping the line intensity of tracer molecules to the H_2 column density is obfuscated by the fact that the dependence of the conversion factor on ISM properties, e.g. metallicity or interstellar radiation field, is not well understood (Glover & Mac Low 2010). In addition, radiative transfer effects need to be carefully modeled (e.g., Narayanan et al. 2008, 2010).

Numerical simulations offer a different route to studying the $\Sigma_{\rm SFR} - \Sigma_{\rm H_2}$ relation. What are their requirements? First, the numerical code needs to follow self-consistently the formation and destruction of H_2. This implies a resolution of 100 pc or better, an implementation of cooling down to a few tens of Kelvin and, also, radiative transfer of the Lyman-Werner bands (at least in some approximate form), in order to correctly capture the impact of the interstellar radiation field on the H_2 dissociation.

Secondly, the code needs a recipe for star formation. The accumulating evidence in favor of a universal initial stellar mass function (Bastian et al. 2010) indicates that star formation on small scales, i.e. within star forming clumps and cores within molecular clouds, is largely decoupled from the ISM properties on larger scales. In particular, observations show that the average star formation efficiency per free fall time is $\sim 0.005 - 0.01$, independently of scale, once the densities of molecular clouds are reached (e.g., Krumholz & Tan 2007, but see also Murray 2010; Feldmann & Gnedin 2010). A natural approach is therefore to couple the star formation on scales of individual molecular clouds directly to the density of molecular hydrogen assuming the formation and destruction of H_2 can be modeled reliably. Consequently, the approach we use in our simulations is to relate the SFR to the H_2 density *on small scales* (~ 60 pc) via the following equation (Gnedin et al. 2009):

$$\dot{\rho}_* = \epsilon_{\rm SFR} \frac{\rho_{\rm H}}{\tau_{\rm SFR}} f_{\rm H_2}, \qquad (1)$$

here $\dot{\rho}_*$ is the *instantaneous* SFR density, $\rho_{\rm H}$ is the hydrogen mass density, $f_{\rm H_2}$ the H_2 fraction, and $\epsilon_{\rm SFR}$ and $\tau_{\rm SFR}$ denote the star formation efficiency and the star formation time-scale (see equation 2 below), respectively. Our simulations use $\epsilon_{\rm SFR} = 0.005$. This value, which is consistent with small scale observations (Krumholz & Tan 2007), ensures that the normalization of the $\Sigma_{\rm SFR} - \Sigma_{\rm H_2}$ relation on kpc scales is similar in simulations and observations.

On which grounds would we actually expect to see any dependence of slope, intercept and scatter of the $\Sigma_{\rm SFR} - \Sigma_{\rm H_2}$ relation on environmental parameters such as metallicity or interstellar radiation field? The H_2 abundance is strongly affected by the amount of dust shielding from the UV radiation and, consequently, a lower metallically and/or larger radiation field will increase the required density for H_2 (and consequently stars) to form. We will show that a non-linear relation between $n_{\rm H_2}$ and the SFR on small scales can have a significant impact on the slope, intercept and scatter of the $\Sigma_{\rm SFR} - \Sigma_{\rm H_2}$ relation measured on large ($\sim$ kpc) scales. Another important, and so far often neglected quantity, is the scatter in the $\Sigma_{\rm SFR} - \Sigma_{\rm H_2}$ relation. While some scatter may be due to observational measurement uncertainties it is clear that any environmental dependence of the $\Sigma_{\rm SFR} - \Sigma_{\rm H_2}$ relation will translate into a galaxy-to-galaxy variation and, in combined data sets, to scatter. Furthermore, the observed $\Sigma_{\rm SFR} - \Sigma_{\rm H_2}$ relation is measured on large scales (spatial averaging) using time averaged SFRs. In addition to any intrinsic scatter the averaging may induce a scale-dependent scatter. The comparison of this scatter with that measured in observations may help to constrain the interplay between molecular gas and star formation on small scales.

TABLE 1
Overview of the simulations discussed in this work.

$n_{\rm c}$ [cm^{-3}]	$Z/Z_\odot$	$U_{\rm MW}$	resolution [pc]	#
50	0.1, 0.3, 1	0.1,1,10,100	65	12
10^3, 10^6	1	0.1	65	2
10^3, 10^6	0.1	100	65	2
50	1	1	32	1
50	1	1	125	1

The layout of the paper is as follows. In §2 we briefly describe the setup of our numerical experiments. We then show in §3.1 the predicted dependence of the slope, intercept and scatter of the $\Sigma_{\rm SFR} - \Sigma_{\rm H_2}$ relation on metallicity and interstellar radiation field. The scale dependence of the scatter is studied in §3.2. We discuss our findings in §4 and conclude in §5.

2. SIMULATIONS

A detailed description of the set of performed simulations can be found in Gnedin & Kravtsov (2010a). All simulations are run with the Eulerian hydrodynamics + N-body code ART (Kravtsov et al. 1997, 2002), that uses an adaptive mesh refinement (AMR) techique to achieve high spatial (and time) resolution in the regions of interested (here: regions of high baryonic density). First, we ran an initial cosmological, hydrodynamical simulation down to $z = 4$. This simulation follows a Lagrangian region that encloses five virial radii of a typical L_* galaxy (halo mass $\sim 10^{12}\ M_\odot$ at $z = 0$) within a box of 6 comoving Mpc/h. The mass of dark matter particles in the high resolution Lagrangian patch is $1.3 \times 10^6 M_\odot$ and the spatial resolution is 65 pc at $z = 3$ in physical coordinates. We adopt the following cosmological parameters $\Omega_{\rm matter} = 0.3$, $\Omega_\Lambda = 0.7$, $h = 0.7$, $\Omega_{\rm baryon} = 0.043$, $\sigma_8 = 0.9$. This initial, fully self-consistent simulation is consequently continued for additional ~ 600 Myr before it is analyzed, but now with metallicities and UV fields fixed to a specific, spatially uniform value. At this time, the mass of the simulated halo is $\approx 4.2 \times 10^{11}\ M_\odot$. We have run a grid of simulations with three different metallicities $Z = 0.1, 0.3, 1.0$ (in units of $Z_\odot = 0.02$) and four different values of the interstellar radiation field $U_{\rm MW} = 0.1, 1, 10, 100$. The parameter $U_{\rm MW} = J/J_{\rm MW}$ specifies the strength of the interstellar radiation field in units of the radiation field of the Milky Way at 1000Å: $J_{\rm MW} = 10^6$ photons cm^{-2} s^{-1} ster^{-1} eV^{-1} (Draine 1978; Mathis et al. 1983). We continued one of our simulations ($Z/Z_\odot = 1$, $U_{\rm MW} = 1$) for additional 400 Myr and found no significant changes in the $\Sigma_{\rm SFR} - \Sigma_{\rm H_2}$ relation. This indicates that the predictions of our simulations should

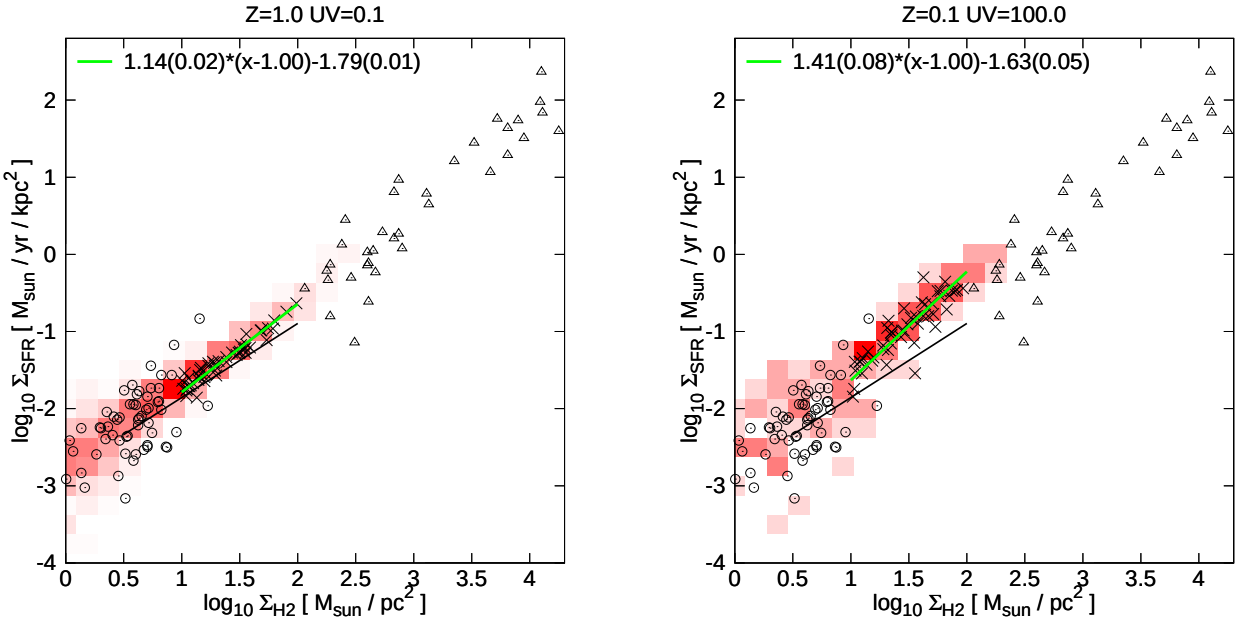

FIG. 1.— The $\Sigma_{\rm SFR} - \Sigma_{\rm H_2}$ relation on the kpc scale. Left panel: $Z = Z_\odot$, $U_{\rm MW} = 1$. Right panel: $Z = 0.1\,Z_\odot$, $U_{\rm MW} = 100$. Stellar and H_2 masses are measured within cubical cells of $l = 1$ kpc box length. Surface densities are estimated by dividing each mass by l^2. SFR are averaged over 20 Myrs. The simulation results are shown as the red shaded region (two-dimensional histogram of all cells) and as crosses (a random sample of 50 cells with surface density in the range $10 < \Sigma_{\rm H_2}/M_\odot{\rm pc}^{-2} < 100$). The solid green line is the result of a bisector regression of all cells with $10 < \Sigma_{\rm H_2}/M_\odot{\rm pc}^{-2} < 100$ and $0.01 < {\rm SFR}/M_\odot{\rm yr}^{-1}{\rm kpc}^{-2} < 1$. The regression parameters, slope and intercept, are shown on the top left. Also shown (in brackets) are the regression errors, estimated via bootstrapping. The black circles and triangles correspond to the normal spiral and star bursting sample, respectively, of Kennicutt (1998b). The solid black line is the average $\Sigma_{\rm SFR} - \Sigma_{\rm H_2}$ relation found in Bigiel et al. (2008). The $\Sigma_{\rm SFR} - \Sigma_{\rm H_2}$ relation in the right panel has a steeper slope, a higher normalization and a larger scatter than in the left panel.

also hold for redshifts $z \lesssim 3$, at least unless/until ISM properties change radically. In total, we ran a set of 18 simulations in order to explore the effect of varying metallicity, radiation field and density threshold on the $\Sigma_{\rm SFR} - \Sigma_{\rm H_2}$ relation (see Table 1).

The molecular hydrogen fraction $f_{\rm H_2}$ is computed self-consistently, including a chemical network comprised of 6 species and radiative transfer of the UV continuum and the Lyman-Werner bands (Gnedin & Kravtsov 2010a). If the average density in a simulation cell is smaller than the density typical for molecular clouds we have to revert to a 'subgrid' interpretation of the H_2 fraction. In this case we assume that the fraction $f_{\rm H_2}$ corresponds to the (mass) fraction of hydrogen in individual (unresolved) molecular clouds. Hence, the star formation timescale is naturally given by the minimum of (i) the free-fall time corresponding to the average density in the cell and (ii) the free fall time corresponding to the minimum density of molecular clouds that form stars $n_{\rm c}$, i.e.

$$\tau_{\rm SFR} = \min[\tau_{\rm ff}(n_{\rm H}), \tau_{\rm ff}(n_{\rm c})], \qquad (2)$$

We stress that for densities smaller than $n_{\rm c}$ the relation between SFR and H_2 abundance is linear, while it becomes non-linear for larger densities, because $\tau_{\rm ff}(n_{\rm H}) \propto n_{\rm H}^{-1/2}$. A non-linear steepening of the $\Sigma_{\rm SFR} - \Sigma_{\rm H_2}$ relation at $\Sigma_{\rm H_2} > 100 M_\odot$ pc^{-2} is motivated by theoretical studies (e.g., Krumholz et al. 2009b), but not yet confirmed by observations. We therefore explore the case in which $n_{\rm c} = 50$ cm^{-3}, i.e. close to the typical average density of molecular clouds ($\sim 100 - 200$ cm^{-3}), but also discuss the possibility of much larger thresholds such as $n_{\rm c} = 10^3$ cm^{-3} and $n_{\rm c} = 10^6$ cm^{-3}. Since our simulations do not capture densities of $\gtrsim 10^5$ cm^{-3}, a threshold above this value effectively corresponds to a linear SFR - H_2 relation on small scales.

We note that the approach described by (1) and (2) does not introduce intrinsic scatter. We discuss in §3.2 how such an intrinsic scatter would propagate from the ~ 100 pc to the $\sim$ kpc scales.

Instantaneous SFRs are computed directly using equations (1) and (2). SFRs that are averaged over time T are calculated by counting the number of stars in a cube of given scale with ages below T. Unless otherwise noted, we use $T = 20$ Myr, but we have explicitly checked that our results do not change significantly if larger averaging times are used (up to $T = 200$ Myr). In order to put this into context: observations based on UV luminosities in the wavelength range 1250-2800 Å correspond to an averaging time of ~ 100 Myr, SFR estimates based on nebular emission lines, such as $H\alpha$, correspond to $T \sim 10$ Myr, while SFR estimates based on the FIR continuum (e.g. 24 μm) can vary in the range 10 - 100 Myr (see, e.g., Kennicutt 1998a).

When we talk about the spatial density on a given scale l we simply refer to the amount of mass within a cube of size l. In order to convert from a spatial to a surface density we multiply the spatial density by l. We note that we do not use the surface density on the smallest (~ 60 pc) scale. The smallest value of l is therefore ~ 125 pc.

3. RESULTS

3.1. *Dependence on metallicity and UV field*

In Fig. 1 we plot and compare the $\Sigma_{\rm SFR} - \Sigma_{\rm H_2}$ relation for (a) solar metallicity and $U_{\rm MW} = 0.1$, and (b)

$Z/Z_\odot = 0.1$ and $U_{\rm MW} = 100$. Measured over the range $10 < \Sigma_{\rm H_2}/M_\odot{\rm pc}^{-2} < 100$, the slope of the relation in case (a) is $\sim 1.14 \pm 0.02$, the SFR at a surface density $\Sigma_{\rm H_2} = 10\ M_\odot\ {\rm pc}^{-2}$ is 0.016 $M_\odot\ {\rm yr}^{-1}\ {\rm kpc}^{-2}$ and the scatter of $\log_{10}$ SFR around the best fit is 0.10 dex. The slope is slightly steeper than the one derived from CO measurements ($\sim 0.96 \pm 0.07$; Bigiel et al. 2008). The use of a constant conversion factor between CO intensity and H_2 surface density may, at least partially, explain an observed slope below unity (Feldmann et al. 2010 in prep). As anticipated the choice $\epsilon_{\rm SFR} = 0.005$ leads to a normalization of the simulated $\Sigma_{\rm SFR} - \Sigma_{\rm H_2}$ relation that is close to what is found in observations, once observational data is mapped to the same initial stellar mass function (IMF). In case (b) the slope is significantly steeper ~ 1.4, the SFR at a surface density $\Sigma_{\rm H_2} = 10\ M_\odot\ {\rm pc}^{-2}$ higher (0.023 $M_\odot\ {\rm yr}^{-1}\ {\rm kpc}^{-2}$) and the scatter is larger (0.18 dex).

In Fig. 2 we plot the slope, intercept and scatter of the $\Sigma_{\rm SFR} - \Sigma_{\rm H_2}$ relation, spatially averaged over 1 kpc, for a grid of environmental parameters. The figure shows that the slope, intercept and scatter are systematically changing as a function of Z and $U_{\rm MW}$. A bi-parametric regression (using Z and $U_{\rm MW}$ as independent variables) captures the change in slope and scatter very well. The regression parameters are given in the legend of the figure. A word on the terminology: We refer to the scale at which equations (1) and (2) are applied as "small scales" (~ 60 pc in our simulations). By contrast, we refer to the scales on which the slope and intercept of the $\Sigma_{\rm SFR} - \Sigma_{\rm H_2}$ are measured as "large scales" ($\sim$ kpc in this study).

- Fig. 2 shows that the use of time-averaged SFRs introduces the *dominant* amount of scatter in the $\Sigma_{\rm SFR} - \Sigma_{\rm H_2}$ relation on large scales. Specifically, as the first two panels in the rightmost column demonstrate, the scatter in the relation is significantly larger ($\sim 0.1 - 0.2$ dex) if SFRs are time-averaged, compared with the case that instantaneous SFRs are used ($\sim 0.05 - 0.12$ dex). Time averaging creates scatter because H_2 surface densities are measured instantaneously while the SFRs are averaged over some past time interval.

- However, the use of time averaged SFRs is not the only source of scatter. The important point to realize is that equation (1) depends both on the H_2 density ($\rho_{\rm H_2} = \rho_{\rm H} f_{\rm H_2}$) *and* the hydrogen density $\rho_{\rm H}$ (via $\tau_{\rm SFR}$). Hence, on small scales, a scatter in the hydrogen density at *fixed* H_2 density translates into a scatter of SFR at fixed H_2 surface density. The value of the threshold $n_{\rm c}$ affects this type of scatter in a crucial way. If $n_{\rm c}$ is very large (much larger than the peak in the mass-weighted distribution function of molecular hydrogen) then the SFR does not depend explicitly on $\rho_{\rm H}$ (since $\tau_{\rm SFR} = \tau_{\rm ff}(n_{\rm c})$) and, consequently, no scatter is generated. Similarly, for hydrogen densities above a certain limit, $n_{\rm fm}$, (e.g., > 300 cm^{-3} for $U_{\rm MW} = 100$, $Z/Z_\odot = 0.1$ or > 10 cm^{-3} for $U_{\rm MW} = 0.1$, $Z/Z_\odot = 1$) the gas is fully molecular and, hence, $\rho_{\rm H}$ and $\rho_{\rm H_2}$ are 1:1 related (see, e.g., Gnedin et al. 2009). If $n_{\rm H} > n_{\rm fm}$ no scatter is produced on the level of a single cell, but scatter can still arise on *larger* scales as cell with different properties are added. To clarify this point, let us assume that we add the SFRs and H_2 densities from, e.g., two cells A and B. Consider now the following scenarios. First, let cell A have a density below $n_{\rm c}$ and cell B a density above $n_{\rm fm}$. Second, let us redistribute the hydrogen and H_2 masses such that *both* cells have a density below $n_{\rm c}$ (this might not be possible in all cases). Although in both cases the H_2 density is the same, the SFRs are higher in the first case.

- The mechanism that we just described explains the *existence* of scatter, provided $n_{\rm c}$ is sufficiently low (see the third column of Fig. 2). However, we have not discussed why there is a *trend* of scatter with Z and $U_{\rm MW}$. The origin of this trend can be understood from Fig. 3, where we show a 2-dimensional histogram of the mass-weighted H_2 distribution as function of small scale hydrogen density and large scale H_2 surface density. Note that only H_2 surface densities in the range $10 < \Sigma_{\rm H_2}/M_\odot{\rm pc}^{-2} < 100$ are the subject of this paper. The figure shows that the fraction of H_2 mass that is in cells with hydrogen densities above a given threshold (in the range $\sim 10 - 100$ cm^{-3}) increases with decreasing Z and increasing UV. Hence, more of the H_2 mass participates in producing scatter and the overall scatter increases.

- Fig. 2 also shows that there is a dependence of the intercept of the $\Sigma_{\rm SFR} - \Sigma_{\rm H_2}$ relation on Z and $U_{\rm MW}$, provided $n_{\rm c}$ is sufficiently small (see left and middle panel in the top & middle row). How do we understand this result? As we just pointed out an increase in the radiation field and/or a decrease in the metallicity shifts the peak of the mass weighted H_2 density distribution towards higher densities (see Fig. 3). Specifically, the figure shows that for $U_{\rm MW} = 0.1$ and $Z/Z_\odot = 1$ only cells with hydrogen densities in the range of $\sim 3 - 100$ cm^{-3} contain molecular hydrogen and thus contribute to the SFR. On the other hand, if $U_{\rm MW} = 100$ and $Z/Z_\odot = 0.1$, only cells with hydrogen densities in the range of $100 - 500$ cm^{-3} contribute to star formation. Furthermore, in the regime in which hydrogen gas is fully molecular and $n_{\rm H} > n_{\rm c}$ the SFRs scale as $\propto n_{\rm H}^{1.5}$. This non-linear scaling leads to an increase in the SFR with decreasing Z and increasing $U_{\rm MW}$ *at a given* large scale H_2 surface density. In other words, the large scale SFRs depend not only on the large scale H_2 surface densities, but also on the distribution function of $n_{\rm H}$ on small scales.

- A related mechanism leads to a dependence of the slope on Z and $U_{\rm MW}$. Fig. 3 demonstrates that the average (small scale) density of cells containing most of the H_2 mass increases with increasing (large scale) hydrogen surface density $\Sigma_{\rm H_2}$. Again, due to the non-linearity of (1) the SFR grows faster than $\Sigma_{\rm H_2}$, which steepens the slope beyond a slope of unity. Let us emphasize this point again. *The slope of the* $\Sigma_{\rm SFR} - \Sigma_{\rm H_2}$ *relation on kpc scales can vary and depends on the actual* H_2 *density distribution as function of* H_2 *surface density.* In par-

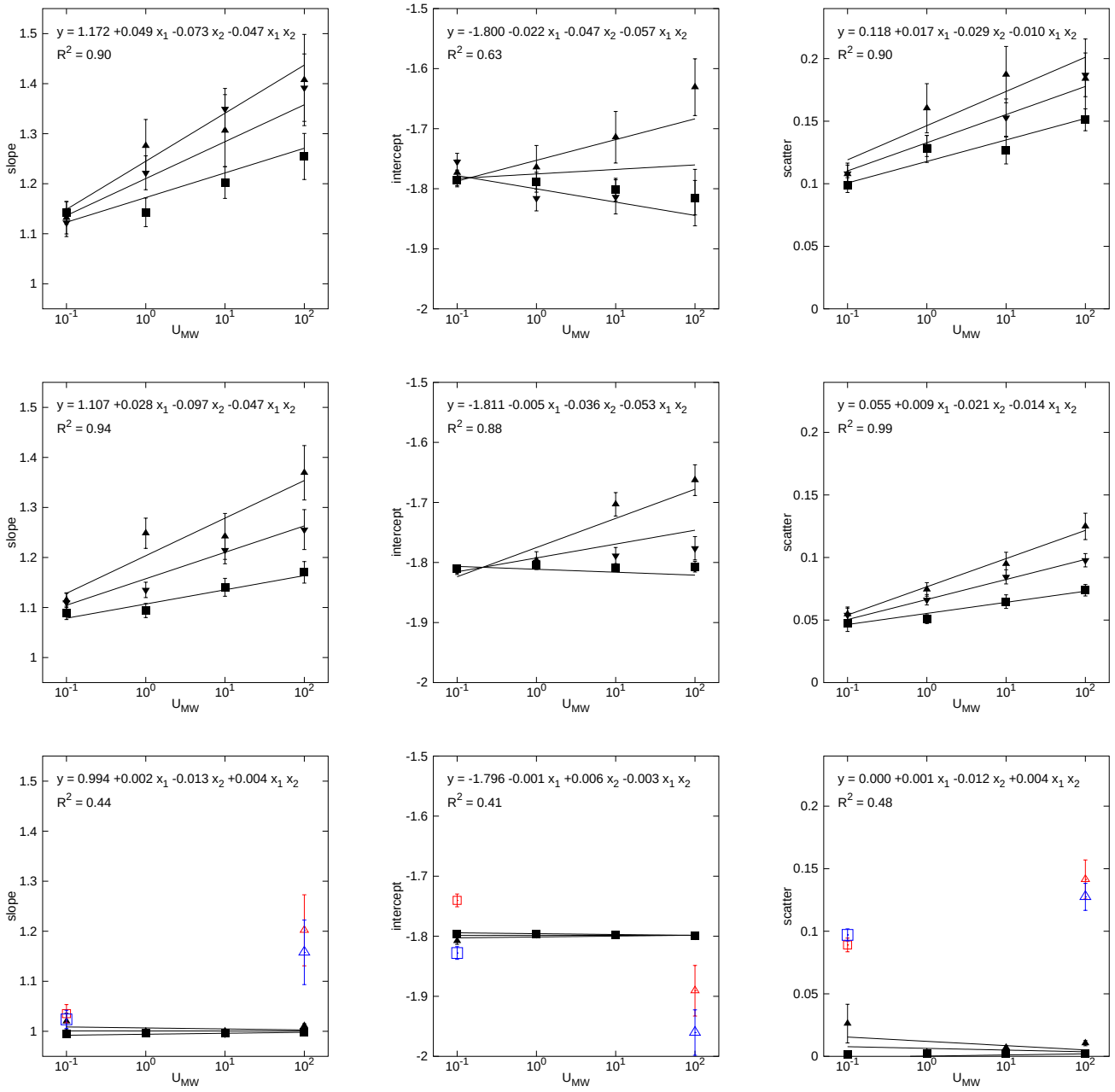

FIG. 2.— The dependence of slope, intercept and scatter on metallicity and interstellar radiation field. The *first* row shows (from left to right) the slope, the intercept and the scatter of the $\Sigma_{\rm SFR} - \Sigma_{\rm H_2}$ relation (averaged over kpc scales) as function of the radiation field, $U_{\rm MW}$ (x-axis), and for different metallicities ($Z/Z_\odot = 1$ (square), 0.3 (downward pointing triangle), and 0.1 (upward pointing triangle)). SFR are averaged over 20 Myr and the minimum cloud density is $n_{\rm c} = 50$ cm^{-3}. Slope, intercept and scatter are computed from a bisector regression of the $\Sigma_{\rm SFR} - \Sigma_{\rm H_2}$ relation as described in the caption of Fig. 1. To highlight the trends with Z and $U_{\rm MW}$ we also performed a two-parametric regression of slope, intercept and scatter as a function of Z and $U_{\rm MW}$ (regression parameters and the square of the correlation coefficient are shown at the top of each panel; $x_1 = \log_{10} U_{\rm MW}$, $x_2 = \log_{10} Z$). The *middle* row shows the same quantities as the top row, but using instantaneous SFR. The *bottom* row shows again the same quantities, but for a larger threshold density $n_{\rm c}$. Specifically, the filled black symbols and lines use instantaneous SFRs and $n_{\rm c} = 1000$ cm^{-3}, while the empty symbols use time-averaged SFRs and $n_{\rm c} = 1000$ cm^{-3} (small red symbols) and $n_{\rm c} = 10^6$ cm^{-3} (large blue symbols), respectively. We note that whenever $n_{\rm c} > 50$ cm^{-3} the star formation efficiencies are reduced by $\sqrt{n_{\rm c}/50}$ (see equations 1 and 2) in order to ensure the correct normalization of the $\Sigma_{\rm SFR} - \Sigma_{\rm H_2}$ relation.

ticular, the slope is not bounded by the small scale exponent of 1.5. In the most extreme case, all the H_2 that resides in a region of a given surface density Σ_{H_2} is located within a single molecular cloud of extreme density. The SFRs are then very large, because the free-fall time of such a cloud is very small.

- While the time averaging of the SFRs generates most of the scatter in the $\Sigma_{SFR} - \Sigma_{H_2}$ relation, the trends of slope and scatter with Z, and U_{MW} are largely driven by the non-linear coupling between SFR and H_2 density. This can be clearly seen in the last row of Fig. 2. If $n_c = 10^6$ cm^{-3}, the slope of the $\Sigma_{SFR} - \Sigma_{H_2}$ relation changes only between 1.03 ($Z/Z_\odot = 1$, $U_{MW} = 0.1$) and 1.16 ($Z/Z_\odot = 0.1$, $U_{MW} = 100$) and the scatter increases only from 0.09 dex to 0.12 dex. We discuss the dependence of the scatter on ISM properties further in the next section.

- If SFRs are measured instantaneously *and* the small scale relation between star formation rate density and H_2 density is linear (i.e. n_c is large), then the slope reduces to exactly unity, any dependence of the intercept on metallicity or radiation field is eliminated and the scatter vanishes (at least as long as there are no other sources of scatter, see §3.2).

We conclude that slope, intercept and scatter of the $\Sigma_{SFR} - \Sigma_{H_2}$ relation averaged on kpc scales can change systematically with metallicity and radiation field. The origin of this behavior lies in the (assumed) non-linear relation between SFR and H_2 density on small scales. On contrast, the use of time-averaged SFRs is responsible for most of the scatter in the relation.

3.2. *Dependence on averaging scale*

Observational studies show that the $\Sigma_{SFR} - \Sigma_{H_2}$ relation has larger scatter on smaller scales (Verley et al. 2010; Onodera et al. 2010; Danielson et al. 2010). Specifically, recent observations of CO, Hα and 24μm emission in M33 have been used to argue that the $\Sigma_{SFR} - \Sigma_{H_2}$ relation "breaks down" on a scale of ~ 100 pc. It has been suggested that the drifting of newly formed star clusters or the difference in evolutionary stages of molecular clouds / star clusters could be responsible (Onodera et al. 2010). Given the limited range of measured gas surface densities it is plausible that this "break-down" is merely a manifestation of a very large scatter that may arise from a variety of sources. In Onodera et al. (2010) the studied range of surface densities is approximatively $1 M_\odot \mathrm{pc}^{-2} < \Sigma_{H_2} < 10 M_\odot \mathrm{pc}^{-2}$. By contrast, the average gas surface density of GMC measured on scales of a few tens of pc in M33 is $\sim 120 M_\odot \mathrm{pc}^{-2}$ (Rosolowsky et al. 2003), roughly similar to what is found in the Milky Way (Solomon et al. 1987; Heyer et al. 2009). Hence, H_2 gas surface densities below $\lesssim 10 M_\odot/\mathrm{pc}^2$ measured on 100 pc scales must correspond to the outskirts of GMCs, not to GMCs themselves. This by itself may be responsible for a substantial fraction of the measured scatter. We, instead, will focus on a 10 times larger range of H_2 surface densities, namely $10 M_\odot/\mathrm{pc}^2 < \Sigma_{H_2} < 100 M_\odot/\mathrm{pc}^2$ for scales

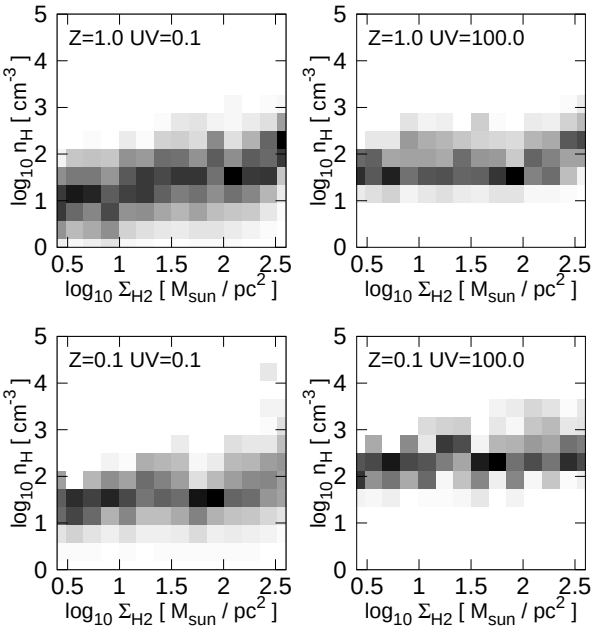

FIG. 3.— The distribution of H_2 mass in cells with hydrogen density n_H as function of large scale (1 kpc) H_2 surface density. Each vertical bin (corresponding to a certain H_2 surface densities) is normalized independently to the total mass of H_2 in the bin (black = all the H_2 mass in the given surface density bin sits at a certain cell scale (65 pc) hydrogen density n_H). The panels from top left to bottom right correspond to four different simulations with $Z = Z_\odot$, $U_{MW} = 0.1$ (top left), $Z = Z_\odot$, $U_{MW} = 100$ (top right), $Z = 0.1\,Z_\odot$, $U_{MW} = 0.1$ (bottom left), $Z = 0.1\,Z_\odot$, $U_{MW} = 100$ (bottom right).

from kpc down to 100 pc. Although we do not aim at a precise quantitative comparison with observations (we have some reasons to believe that our simulations should underestimate the scatter on small scales somewhat, see below), we will discuss qualitative predictions of the simulations, their limitations and the resulting implications.

In Fig. 4 we show the scatter of the $\Sigma_{SFR} - \Sigma_{H_2}$ relation as function of scale from 1 kpc down to ~ 100 pc. The first thing we notice is that the scatter due to time averaging alone (red lines, triangles) increases with decreasing scale, while the scatter solely due to the threshold density n_c (blue lines, diamonds) remains roughly scale independent. The origins of the different types of scatter have been discussed in the last section. Unless there are other intrinsic sources of scatter the figure shows that the scatter on all scales arises mainly from the time averaging of the SFR and, consequently, is not related to the H_2 density pdf. This is not an artifact of the particular SFR averaging time used. We varied the SFR averaging time scales between 20 and 200 Myrs and found no substantial change in the amount of scatter, as long as low SFR outliers (> 3 sigma) are excluded[5].

The figure also shows that the scatter due to the SFR time averaging alone depends to a small extent on U_{MW} and Z. This result can be rephrased in terms of a duty fraction, which we define as the fraction of time (the relevant time scale is the SFR averaging time) during which the H_2 density within the considered cell is close to its

[5] If not excluded these outliers do increase the scatter somewhat (by ~ 0.1 dex) when averaging over 200 Myr instead of 20 Myr.

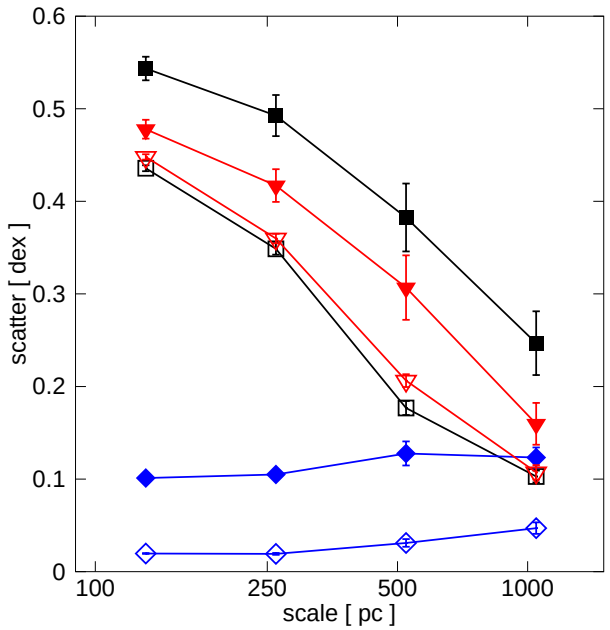

FIG. 4.— The dependence of the scatter in the $\Sigma_{\rm SFR} - \Sigma_{\rm H_2}$ relation on the averaging scale. The scatter in the $\Sigma_{\rm SFR} - \Sigma_{\rm H_2}$ relation has been derived assuming either (i) time averaged SFR (20 Myr) and a minimum cloud density of $n_{\rm c} = 50$ cm^{-3} (black squares), (ii) time averaged SFR and $n_{\rm c} = 10^6$ cm^{-3} (red triangles), or (iii) instantaneous SFR and $n_{\rm c} = 50$ cm^{-3} (blue diamonds). The scatter is computed with an ordinary least squares regression of the SFR as function of H_2 surface density in the range $10 < \Sigma_{\rm H_2}/M_\odot{\rm pc}^{-2} < 100$. Errors are computed via bootstrapping. Empty symbols correspond to solar metallicity and $U_{\rm MW} = 0.1$, while filled symbols refer to $Z = 0.1\,Z_\odot$ and $U_{\rm MW} = 100$. Simulations with intermediate values of metallicity and UV field lie in between.

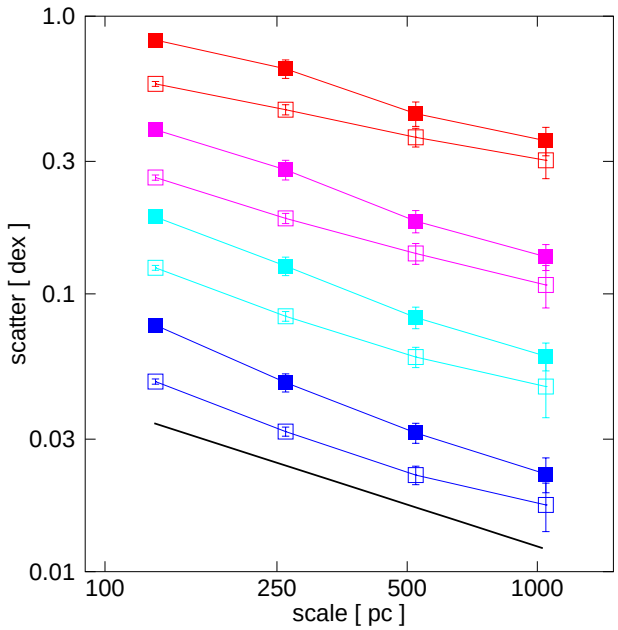

FIG. 5.— The propagation of scatter in the $\Sigma_{\rm SFR} - \Sigma_{\rm H_2}$ relation from small to large scales. A scatter in $\log_{10}({\rm SFR}[M_\odot{\rm yr}^{-1}])$ of (from bottom to top) 0.1 (blue lines), 0.25 (cyan lines), 0.5 (magenta lines) and 1 (red lines) is inserted at the resolution scale (65 pc) of the simulation. The black line at the bottom shows a power law: scatter $\propto$ scale$^{-0.5}$. The scatter in the $\Sigma_{\rm SFR} - \Sigma_{\rm H_2}$ relation is measured in the range $10 < \Sigma_{\rm H_2}/M_\odot{\rm pc}^{-2} < 100$. Instantaneous SFRs and a minimum cloud density of 10^6 cm^{-3} are used in order to suppress other sources of scatter. Filled (empty) symbols correspond to the simulation with $Z = 0.1\,Z_\odot$, $U_{\rm MW} = 100$ ($Z = Z_\odot$, $U_{\rm MW} = 0.1$).

time averaged value. A duty fraction of unity does not introduce scatter on small scales, as it means that within the SFR averaging time the H_2 content within the cell remains constant. Fig. 4 then shows that the duty fraction decreases with increasing radiation field/decreasing metallicity, hence leading to larger scatter. One interpretation of the reduced duty fraction is that stronger $U_{\rm MW}$ and/or lower Z reduce the life times of molecular clouds. An alternative possibility is that molecular clouds live as long as before, but molecular cloud formation is rarer.

Another potential contributor to the scatter on small scales is the velocity spread of young stellar clusters and of the stars within the cluster. This effect is not modeled adequately in the simulation because we do not resolve individual cluster members, but rather obtain one 'star particle' for each cluster that initially moves with the average velocity of the gas. On scales $\gtrsim 100$ pc this effect plays only a small role presumably, as the typical distance that stars travel within 20 Myr is of the order of ~ 100 pc (assuming a rms velocity of ~ 5 km/s). Some scatter on large scales may arise from high-velocity runaway stars (Blaauw 1961; Stone 1991).

The decline of the scatter with increasing averaging scale is obviously related to the spatial averaging over a larger number of resolution elements $N_{\rm res}$. If there were no correlation in the H_2 content of neighboring cells we would expect a scaling proportional to $\sqrt{N_{\rm res}}$, where $N_{\rm res} \propto l^3$ if the H_2 is filling the volume relatively uniformly, or $\propto l^2$ if the H_2 is confined to a disk. However, the scale dependence shown in Fig. 4 seems to be much shallower.

In order to address this question, we show in Fig. 5 the result of a simple experiment. We insert a log-normal scatter (in the SFRs) at the 65 pc scale by treating the SFR as a log-normal random variable, with a mean given by equation 1 and a standard deviation of 0.1 to 1 dex. We see that the scatter decreases with increasing averaging scale. A fit to the average of all data points shows that the scatter behaves as

$$\sigma_l = \sigma_{\rm 1kpc}\,(l\,[{\rm kpc}])^{-\alpha}\,,$$

with $\alpha \approx 0.5$. The precise value of the exponent depends slightly on the environmental properties of the gas. Using the data points shown in Fig. 5 we obtain $\alpha = 0.52 \pm 0.04$ for $Z = 0.1$, $U_{\rm MW} = 100$, and $\alpha = 0.43 \pm 0.04$ for $Z = 1$, $U_{\rm MW} = 0.1$. This implies that on average $N_{\rm res} \propto l$. Another way of saying this is that the H_2 distribution in cells with a given H_2 surface density in the range $10 < \Sigma_{\rm H_2}/M_\odot p^{-2} < 100$ is effectively one-dimensional. Although this does not mean that the H_2 is necessarily arranged in a one-dimensional configuration, this is what one would expect if most of the star formation takes places in spiral waves in disk galaxies. On the other hand, in flocculent disks, H_2 masses that are smoothed on scales of > 100 pc should be less correlated and we

would therefore expect a steeper scaling closer to $\propto l^{-1}$. We note that the scatter that originates in the time averaging of star formation (see Fig. 4) follows roughly the $l^{-0.5}$ scaling.

Let us now consider the case in which a scatter $\tilde{\sigma}_l$ is inserted on scale l (we assume a set of discrete scales that change by a factor 2). If the different scatter contributions add in quadrature the total scatter σ_l on a given scale l is simply given by

$$\sigma_l^2 = \tilde{\sigma}_l^2 + \frac{1}{2^{2\alpha}}\tilde{\sigma}_{l/2}^2 + \frac{1}{4^{2\alpha}}\tilde{\sigma}_{l/4}^2 + \dots \quad (3)$$

$$= \tilde{\sigma}_l^2 + \frac{1}{2^{2\alpha}}\sigma_{l/2}^2. \quad (4)$$

With knowledge of α this equation allows the computation of the amount of scatter $\tilde{\sigma}_l$ that is introduced on scale l from the measurement of the scatter on scale l and $l/2$. Presumably, different physical mechanism may introduce different amounts of scatter on different scales. Studying the scale dependence of the scatter may therefore be helpful to uncover the responsible physical mechanism(s). Our simulations also predict that the scatter should never increase by more than 2^α when averaging scales decrease by a factor of 2. We note that our analysis assumes a log-normal distribution in the scatter in the SFR. Scatter sources that do not produce a log-normal scatter may lead to a different scale dependence.

A rather subtle point is that the form of the distribution of scatter can actually have an impact on the measured star formation efficiency per free-fall time used in equation (1). For instance, if the $\Sigma_{\rm SFR} - \Sigma_{\rm H_2}$ relation is scatter-free on some small scale $< l$ and some log-normally distributed scatter is introduced on scale l (with spread σ in $\ln {\rm SFR}$) then the SFR density, $\dot{\rho}_*$, becomes a random variable

$$\dot{\rho}_* = \epsilon_{\rm SFR}\frac{\rho_{\rm H_2}}{\tau_{\rm SFR}}e^{\sigma X},$$

where X is a normal distributed random variable with mean 0 and variance 1. The average SFR density measured on scales $\geq l$ is then given by (assuming $\rho_{\rm H_2}/\tau_{\rm SFR}$ and X are statistically independent):

$$\langle\dot{\rho}_*\rangle = \epsilon_{\rm SFR}\left\langle e^{\sigma X}\right\rangle\left\langle\frac{\rho_{\rm H_2}}{\tau_{\rm SFR}}\right\rangle = \epsilon_{\rm SFR}e^{\frac{1}{2}\sigma^2}\left\langle\frac{\rho_{\rm H_2}}{\tau_{\rm SFR}}\right\rangle$$

That is, the effective star formation efficiency per free fall time measured on scales $\geq l$ is larger by a factor $e^{\frac{1}{2}\sigma^2}$ compared to the star formation efficiency on scales $< l$. A log-normal scatter of, e.g., 0.6 dex will lead to an increase in the star formation efficiency by a factor of ≈ 2.6, which is smaller than the range (0.005-0.02) of observationally determined star formation efficiencies over a variety of density and spatial scales (e.g., Krumholz & Tan 2007; Bigiel et al. 2008; Lada et al. 2010). On the other hand, an intrinsic log-normal scatter of 1 (1.5) dex would increase the star formation efficiency by more than an order (two orders) of magnitude, which seems difficult to reconcile with observations.

4. DISCUSSION

The scatter in the $\Sigma_{\rm SFR} - \Sigma_{\rm H_2}$ relation on the scale of ~ 100 pc has been attributed to the evolution of molecular clouds over their life time (see, e.g., Onodera et al. 2010; Schruba et al. 2010). In this picture young molecular clouds have not yet formed stars, but contain large amounts of H_2 and hence fall "below" the average $\Sigma_{\rm SFR} - \Sigma_{\rm H_2}$ relation. On the other hand, clouds that are near the end of their lives are heavily star forming and/or have lost some fraction of their molecular hydrogen - hence the lie "above" the relation. This picture cannot be reconciled with an H_2-based star formation law of the form of equation (1) as long as the gas consumption time scale $\tau_{\rm SFR}/\epsilon_{\rm SFR}$ is treated as a constant. Hence, this explanation of the scatter in the $\Sigma_{\rm SFR} - \Sigma_{\rm H_2}$ relation implies that $\epsilon_{\rm SFR}/\tau_{\rm SFR}$ has to be a time-dependent quantity. If $\tau_{\rm SFR}$ is approximatively constant, then the star formation efficiency will need to change over the life time of a molecular cloud (e.g., Murray 2010, but see Feldmann & Gnedin 2010).

Our interpretation is different. We show that a large amount of scatter in the $\Sigma_{\rm SFR} - \Sigma_{\rm H_2}$ relation can be explained by the fact that observations do not measure the instantaneous rate of star formation, but rather the number of stars that formed within a finite time interval in the past. Our numerical models predict that the scatter seen on scales of ~ 100 pc should be small ($\lesssim 0.1$ dex) *if* SFR are measured instantaneously. By contrast, if the scatter in the relation is mainly due to an evolving star formation efficiency, the scatter on 100 pc scales should not be strongly diminished if (close to) instantaneous SFR are used.

We note that the particular small-scale model of star formation used in our simulations is based directly on the H_2 density (equation 1). Although this model has been motivated analytically (Krumholz et al. 2009b) and is widely used in numerical simulations (Gnedin et al. 2009) or, more recently, semi-analytic models (Fu et al. 2010), it is important to verify how accurately it describes reality. A potential shortcoming of equation (1) is that it assumes that a fixed mass fraction of molecular hydrogen is available/eligible for star formation. It has been known for a while now that star formation in molecular clouds occurs preferentially in region of high gas density ($n \gtrsim 10^4$ cm^{-3}, see e.g. Lada 1992; Gao & Solomon 2004; Lada et al. 2010). Hence, the SFR should be strongly dependent on the density probability distribution function (pdf) of the gas and not necessarily on the total mass of molecular hydrogen alone.

The density pdf can be expected to depend on details of gas thermodynamics or potential feedback mechanisms (e.g., Wada & Norman 2001; Robertson & Kravtsov 2008), even in a picture in which the turbulence in the ISM is mainly driven by large scale gravitational motions (e.g., Wada & Norman 2001; Tasker & Tan 2009). Hence, if the SFR is in fact regulated by the amount of high density gas (and not by H_2), we can expect to see differences in the SFR on $\sim$ kpc patches as function of Z and $U_{\rm MW}$, even for the same star formation prescription on small scales.

But even if the density pdfs were not significantly changing with Z and $U_{\rm MW}$, the amount of H_2 should. For instance, the total amount of H_2 in the simulated volume changes by a factor $\sim 2-3$ when metallicities and radiation fields are varied in the range $Z/Z_\odot = 0.1 - 1$ and $U_{\rm MW} = 0.1 - 100$. This change in the H_2 mass alone should induce a galaxy-by-galaxy scatter on the order of ~ 0.2 dex. A study of the scatter of the $\Sigma_{\rm SFR} - \Sigma_{\rm H_2}$

relation as function of scale and in regions with different metallicities and UV radiation fields may thus give us, at least in principle, a means to test this picture.

5. CONCLUSIONS

5.1. *The scatter in the* $\Sigma_{\rm SFR} - \Sigma_{\rm H_2}$ *relation*

Our simulations identify and quantify two important sources of scatter. The first is related to the scatter in the H_2 density at fixed gas density, the second arises due to the use of SFR that are time-averaged over tens of Myr. The former source of scatter is relatively independent of spatial scale and is smaller (at least on the considered scales 100 pc - 1 kpc) than the scatter due to SFR time averaging. The latter increases if one goes to smaller scales. Our simulations predict a typical scatter of the order of $\sim 0.4 - 0.6$ dex in $\log_{10}$SFR on ~ 100 pc scales. Intrinsic scatter that is generated on a $\sim$ 100 pc scale is expected to scale approximately as $\propto$ scale$^{-0.5}$. We note that our simulations provide only a lower limit on the expected scatter as function of scale, because some sources of scatter (e.g., the velocity dispersion of clusters and their member stars) are not represented realistically (or at all) in our numerical modeling.

A precise observational determination of the scatter-scale relation, possibly even as a function of ISM environment, and the comparison with theoretical predictions, such as the one presented in this paper, may thus help to identify the physical processes responsible for creating the scatter. Consequently, we argue that the scale dependence of the scatter in the $\Sigma_{\rm SFR} - \Sigma_{\rm H_2}$ relation could become an important diagnostic tool in determining the underlying connection between star formation and H_2 density.

5.2. *The environmental variation of the* $\Sigma_{\rm SFR} - \Sigma_{\rm H_2}$ *relation*

We have shown that even if the star formation rate is tightly coupled to the H_2 density on small scales (see equation 1), the $\Sigma_{\rm SFR} - \Sigma_{\rm H_2}$ relation can vary systematically with metallicity and interstellar radiation field in the studied surface density range $10 < \Sigma_{\rm H_2}/M_\odot{\rm pc}^{-2} < 100$, when averaged on $\sim$ kpc scales.

In particular, the super linear slope of the $\Sigma_{\rm SFR} - \Sigma_{\rm H_2}$ relation depends on the actual H_2 density distribution and on the existence of a non-linear scaling between SFR and H_2 density. The underlying reason for a slope steeper than unity is that the peak of the H_2 density distribution changes systematically with large scale surface density. At larger $\sim$ kpc averaged surface densities more of the molecular gas sits at higher densities, which, due to the non-linear scaling between SFR and density, leads to the super linear steepening of the $\Sigma_{\rm SFR} - \Sigma_{\rm H_2}$ relation.

Similarly, the systematic *change* in the slope with metallicity of the ISM and the interstellar radiation field is a reflection of the change in the H_2 density distribution. For example, in a low metallicity and/or strong radiation field environment the HI to H_2 transition takes places at significantly higher densities and, consequently, a larger fraction of the H_2 mass contributes super-linearly to the SFR. In addition, this implies more star formation at a given H_2 surface density and hence changes the intercept of the $\Sigma_{\rm SFR} - \Sigma_{\rm H_2}$ relation.

The scatter in the $\Sigma_{\rm SFR} - \Sigma_{\rm H_2}$ relation also shows a systematic trend with Z and $U_{\rm MW}$. The precise value of the scatter and the amount it changes with Z and $U_{\rm MW}$ depends on (*i*) the assumed density threshold, $n_{\rm c}$, above which the SFR scales super-linearly with density, and (*ii*) amount of time over which observed SFR are time-averaged. The scatter varies between ~ 0.05 dex ($Z/Z_\odot = 1$, $U_{\rm MW} = 0.1$) and ~ 0.12 dex ($Z/Z_\odot = 0.1$, $U_{\rm MW} = 100$) if $n_{\rm c} = 50$ cm^{-3} and SFRs are measured instantaneously. The trend with Z and $U_{\rm MW}$ is mainly caused by changes in the H_2 and total hydrogen density distributions. On the other hand, if $n_{\rm c}$ is large ($\gtrsim 10^4$ cm^{-3}) and the scatter is generated by the time averaging, then the scatter changes only weakly with Z and $U_{\rm MW}$ (~ 0.09 dex vs. ~ 0.13 dex).

We note that in order to observe a significant change in the $\Sigma_{\rm SFR} - \Sigma_{\rm H_2}$ relation metallicities $\leq 0.3\,Z_\odot$ and interstellar UV fields $U_{\rm MW} \geq 10$ are required. Star forming galaxies at high redshifts should therefore be the natural candidates to test our predictions.

RF thanks A. Leroy and F. Bigiel for stimulating discussions. We are grateful to the Aspen Center for Physics and to the participants and organizers of the workshop "Star Formation in Galaxies: From Recipes to Real Physics". NYG and AVK were supported by the NSF grants AST-0507596 and AST-0708154, and by the Kavli Institute for Cosmological Physics at the University of Chicago through the NSF grant PHY-0551142 and an endowment from the Kavli Foundation. The simulations used in this work have been performed on the Joint Fermilab - KICP Supercomputing Cluster, supported by grants from Fermilab, Kavli Institute for Cosmological Physics, and the University of Chicago. This work made extensive use of the NASA Astrophysics Data System and arXiv.org preprint server.

APPENDIX

RESOLUTION STUDY

In order to test for possible resolution effects we have rerun one of our simulations ($Z = 1$ and $U_{\rm MW} = 1$) at two times better (32 pc) and also two times worse (125 pc) spatial resolution. We show in Fig. A1 the scale dependence of the scatter in the $\Sigma_{\rm SFR} - \Sigma_{\rm H_2}$ relation for the 3 different resolutions (32, 65, 125 pc). As in Fig. 4, we present both the scatter (*i*) due to SFR time averaging (using a high $n_{\rm c}$) and (*ii*) due to the non-linear scaling between SFRs and H_2 density (using instantaneous SFR). We find that the amount of scatter as function of scale is similar in each of the 3 simulations and that there is no apparent significant systematic trend with resolution.

REFERENCES

Bastian, N., Covey, K. R., & Meyer, M. R. 2010, arXiv:1001.2965

Bigiel, F., Leroy, A., Walter, F., Brinks, E., de Blok, W. J. G., Madore, B., & Thornley, M. D. 2008, AJ, 136, 2846

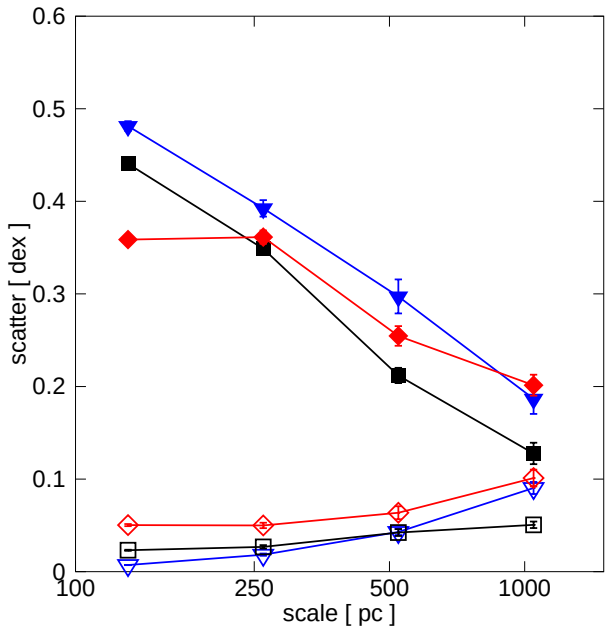

FIG. A1.— The scale dependence of the scatter of the $\Sigma_{\rm SFR} - \Sigma_{\rm H_2}$ relation as in Fig. 4, but now for 3 different spatial resolutions: 125 pc (blue triangles), 65 pc (black squares) and 32 pc (red diamonds). Empty and filled symbols show the scatter due to a low $n_{\rm c}$ and SFR averaging, respectively.

Blaauw, A. 1961, Bull. Astron. Inst. Netherlands, 15, 265
Danielson, A. L. R., Swinbank, A. M., Smail, I., Cox, P., Edge, A. C., Weiss, A., Harris, A. I., Baker, A. J., De Breuck, C., Geach, J. E., Ivison, R. J., Krips, M., Lungdren, A., Longmore, S., Neri, R., & Ocana Flacquer, B. 2010, ArXiv e-prints
Draine, B. T. 1978, ApJS, 36, 595
Feldmann, R., & Gnedin, N. Y. 2010, arXiv:1009.5674
Fu, J., Guo, Q., Kauffmann, G., & Krumholz, M. R. 2010, MNRAS, 1359
Gao, Y., & Solomon, P. M. 2004, ApJ, 606, 271
Glover, S. C. O., & Mac Low, M. 2010, arXiv:1003.1340
Gnedin, N. Y., & Kravtsov, A. V. 2010a, arXiv:1004.0003
—. 2010b, ApJ, 714, 287
Gnedin, N. Y., Tassis, K., & Kravtsov, A. V. 2009, ApJ, 697, 55
Hartwick, F. D. A. 1971, ApJ, 163, 431
Heyer, M., Krawczyk, C., Duval, J., & Jackson, J. M. 2009, ApJ, 699, 1092
Kennicutt, Jr., R. C. 1989, ApJ, 344, 685
—. 1998a, ARA&A, 36, 189
—. 1998b, ApJ, 498, 541
Kravtsov, A. V. 2003, ApJ, 590, L1
Kravtsov, A. V., Klypin, A., & Hoffman, Y. 2002, ApJ, 571, 563
Kravtsov, A. V., Klypin, A. A., & Khokhlov, A. M. 1997, ApJS, 111, 73
Krumholz, M. R., McKee, C. F., & Tumlinson, J. 2009a, ApJ, 693, 216
—. 2009b, ApJ, 699, 850
Krumholz, M. R., & Tan, J. C. 2007, ApJ, 654, 304
Lada, C. J., Lombardi, M., & Alves, J. F. 2010, arXiv:1009.2985
Lada, E. A. 1992, ApJ, 393, L25
Mathis, J. S., Mezger, P. G., & Panagia, N. 1983, A&A, 128, 212
Murray, N. 2010, ArXiv e-prints
Narayanan, D., Cox, T. J., Hayward, C., & Hernquist, L. 2010, arXiv:1005.3020
Narayanan, D., Cox, T. J., Shirley, Y., Davé, R., Hernquist, L., & Walker, C. K. 2008, ApJ, 684, 996
Omont, A. 2007, Reports on Progress in Physics, 70, 1099
Onodera, S., Kuno, N., Tosaki, T., Kohno, K., Nakanishi, K., Sawada, T., Muraoka, K., Komugi, S., Miura, R., Kaneko, H., Hirota, A., & Kawabe, R. 2010, ArXiv e-prints
Robertson, B. E., & Kravtsov, A. V. 2008, ApJ, 680, 1083
Rosolowsky, E., Engargiola, G., Plambeck, R., & Blitz, L. 2003, ApJ, 599, 258
Sanduleak, N. 1969, AJ, 74, 47
Schmidt, M. 1959, ApJ, 129, 243
Schruba, A., Leroy, A. K., Walter, F., Sandstrom, K., & Rosolowsky, E. 2010, arXiv:1009.1651
Solomon, P. M., Rivolo, A. R., Barrett, J., & Yahil, A. 1987, ApJ, 319, 730
Stone, R. C. 1991, AJ, 102, 333
Tasker, E. J., & Tan, J. C. 2009, ApJ, 700, 358
Verley, S., Corbelli, E., Giovanardi, C., & Hunt, L. K. 2010, A&A, 510, A64+
Wada, K., & Norman, C. A. 2001, ApJ, 547, 172
Wong, T., & Blitz, L. 2002, ApJ, 569, 157